An FDTD Method for Analysis of Scattering from Rough Fluid-Fluid Interfaces*

Frank D. Hastings† John B. Schneider‡ Shira L. Broschat‡
Eric I. Thorsos§

February 26, 2001

Abstract

A finite-difference time-domain (FDTD) method for scattering by one-dimensional, rough fluid-fluid interfaces is presented. Modifications to the traditional FDTD algorithm are implemented which yield greater accuracy at lower computational cost. These modifications include use of a conformal technique, in which the grid conforms locally to the interface, and a correction for the numerical dispersion inherent to the FDTD algorithm. Numerical results are presented for fluid-fluid cases modeling water-sediment interfaces. Two different roughness spectra, the single-scale Gaussian roughness spectrum and a multiscale modified power law spectrum, are used. Gaussian results are calculated as a function of the dimensionless parameters kh and kl, where k is the wave number in water, h is the rms surface height, and l is the surface correlation length. For the modified power law spectrum, statistical parameters consistent with an insonification frequency of 7.5 kHz are used. Results are compared with those obtained using an integral equation technique both for scattering from single-surface realizations and for

*Work supported by ONR Code 321OA

†ITT Industries, 45145 Research Place, Ashburn, Virginia 20147 (fdhastings@uswest.net). Work performed while with the School of Electrical Engineering and Computer Science, Washington State University, PO Box 642752, Pullman, WA 99164-2752

‡School of Electrical Engineering and Computer Science, Washington State University, PO Box 642752, Pullman, WA 99164-2752 (schneidj@eecs.wsu.edu, shira@eecs.wsu.edu)

§Applied Physics Laboratory, College of Ocean and Fishery Sciences, University of Washington, 1013 NE 40th St., Seattle, WA 98105 (eit@apl.washington.edu)

Monte Carlo averages of scattering from an ensemble of surface realizations. Scattering strengths are calculated as a function of scattering angle for an incident angle of 70° (20° grazing). The results agree well over all scattering angles for the cases examined.

KEY WORDS: Fluid-fluid interfaces, rough surface scattering, FDTD

1 Introduction

When shear speeds in shallow-water sediment bottoms are relatively slow, a fluid-fluid model is a reasonable approximation for the water-sediment interface. In this paper we present a modified finite-difference time-domain (FDTD) method for calculating the acoustic energy scattered from fluid-fluid interfaces. Simulations performed with this method can be used to study scattering from water-sediment interfaces as well as to benchmark analytic, approximate scattering models which are more readily incorporated into practical models. While no approximations are made to the underlying governing equations, numerical error may be introduced during implementation. Results are compared with those obtained using an integral equation technique which also introduces some numerical error. However, the nature of the numerical error differs for each method. Thus, comparison of the results serves as a means of determining the accuracy of both methods—that is, if the results agree well, it is reasonable to assume that numerical error is negligible for both. The FDTD method is well suited to problems which 1) require broadband analysis or 2) involve inhomogeneous media including multiple layers and discrete scatterers. It is more difficult to implement than an integral equation approach for relatively simple problems such as scattering from an interface separating isovelocity regions, but the extension to complex problems with inhomogeneities in the surrounding environment and multiple velocities does not increase the complexity of the implementation or the computer resource requirements appreciably.

Note that results for both the FDTD and IE methods can be validated independently using successively finer discretizations. In both methods the error is a function of the discretization and goes to zero in the limit of vanishingly small discretization. It thus suffices to show that results do not change (appreciably) with changes in discretization to ensure that accurate results have been obtained. However, such a convergence test is not always feasible and direct comparison of the results from different numerical methods, such as described here, provides another means of validation.

To examine the accuracy of the FDTD technique, scattering strengths are obtained for one-dimensional rough interfaces both for single surface realizations and Monte Carlo averages. Two different roughness spectra, the single-scale Gaussian roughness spectrum and a multiscale modified power law spectrum, and two different sediment bottoms, mud and silty-clay, are used. Shear speeds for both bottom types are negligible, and attenuation is not included. The incident angle is $70°$ measured from the vertical. For the cases examined there are minor differences between the FDTD and IE results for the single surface realizations; these differences are even smaller for the Monte Carlo results. Both numerical methods have small inherent errors because of such things as the use of finite precision numbers and the discretization of continuous quantities. Since the agreement between the two methods is better for Monte Carlo simulations than for individual surfaces, apparently inherent numerical errors manifest themselves nearly randomly, i.e., the errors do not result in a consistent over- or under-prediction of the scattering strength in either method.

In the next section, implementation of the FDTD method for fluid-fluid interfaces is explained. Numerical results for water-sediment interfaces are presented in Sec. 3. A summary of the results of this work is given in Sec. 4.

2 The FDTD Method

In the basic FDTD algorithm, media parameters are specified at discrete locations on a Cartesian grid. Hence, curved boundaries must be approximated using a "staircase." The approximation can be improved, and the associated errors reduced, by decreasing the grid spacing. However, this brute-force approach to improving the model of the interface may be computationally prohibitive. Fortunately, it is possible to modify the basic FDTD algorithm using a conformal technique, for which the grid is locally distorted to conform to the curved boundary [1, 2, 3]. The "local" distortions only occur at cells adjacent to the material interface—cells away from the interface are unaffected. The approach used here is similar to that introduced in [2], but it has been modified for the acoustics problem. Also, the reciprocal borrowing approach introduced in [3] has been used to obtain greater stability and accuracy. (In [1, 3] and [4], the locally conformal technique was presented for interfaces satisfying a Dirichlet boundary condition and is not directly applicable to the fluid-fluid problem.)

Fields propagated in FDTD simulations suffer numerical dispersion such that the phase velocity is less than the true velocity for a given medium. As explained in Sec. 2.1, the amount the numeric phase velocity differs from the true phase velocity depends, at least weakly, on both the frequency and direction of propagation, i.e., the FDTD grid is both dispersive and anisotropic. In this work, the scattering strength at a single frequency is of interest, and energy propagates primarily in the specular direction. Therefore, as discussed in [1], it is possible to incorporate into the FDTD method a correction factor that compensates for numerical dispersion. This correction factor ensures that the numeric wave number in the grid corresponds to the exact wave number for a given frequency and direction of propagation.

2.1 Standard FDTD Equations

The FDTD update equations for acoustic propagation are given in a number of papers including [1, 5, 6, 7]. However, to facilitate development of the local conformal technique, we include them here. The relevant governing differential equations for a two-dimensional (2-D) problem are

$$\frac{\partial p}{\partial t} = -\rho c^2 \left(\frac{\partial v_x}{\partial x} + \frac{\partial v_z}{\partial z} \right) \tag{1}$$

$$\frac{\partial v_x}{\partial t} = -\frac{1}{\rho}\frac{\partial p}{\partial x} \tag{2}$$

$$\frac{\partial v_z}{\partial t} = -\frac{1}{\rho}\frac{\partial p}{\partial z} \tag{3}$$

where p is the pressure, $\vec{v} = v_x \hat{\mathbf{a}}_x + v_z \hat{\mathbf{a}}_z$ is the velocity, ρ is the density, and c is the speed of sound. Approximating the derivatives by finite differences gives the following update equations:

$$\begin{aligned} p^n(i,j) &= p^{n-1}(i,j) - \\ &\quad \frac{\rho c^2 \Delta t}{\delta} \Big[v_x^{n-1/2}(i+1/2,j) - v_x^{n-1/2}(i-1/2,j) + \\ &\qquad v_z^{n-1/2}(i,j+1/2) - v_z^{n-1/2}(i,j-1/2) \Big] \end{aligned} \tag{4}$$

$$v_x^{n+1/2}(i+1/2,j) = v_x^{n-1/2}(i+1/2,j) - \frac{\Delta t}{\rho\delta}\left[p^n(i+1,j) - p^n(i,j)\right] \tag{5}$$

$$v_z^{n+1/2}(i,j+1/2) = v_x^{n-1/2}(i,j+1/2) - \frac{\Delta t}{\rho\delta}\left[p^n(i,j+1) - p^n(i,j)\right] \tag{6}$$

where

$$p^n(i,j) = p(i\Delta x, j\Delta z, n\Delta t) = p(x,z,t) \tag{7}$$

$$v_x^{n+1/2}(i+1/2,j) = v_x\left((i+1/2)\Delta x, j\Delta z, (n+1/2)\Delta t\right) = v_x(x,z,t) \quad (8)$$
$$v_x^{n+1/2}(i,j+1/2) = v_x\left(i\Delta x, (j+1/2)\Delta z, (n+1/2)\Delta t\right) = v_z(x,z,t) \quad (9)$$

The values of ρ and c depend on the medium in which the node falls. The spatial step sizes are Δx and Δz in the x- and z-directions, respectively, and Δt is the temporal step size. Away from the interface, uniform cells are used so that $\Delta x = \Delta z = \delta$. A portion of a typical grid is shown in Fig. 1(a).

In the FDTD algorithm the fields are advanced in a leap-frog manner—current fields are calculated from (known) past fields. For example, at the start of a simulation, (5) and (6) are used to obtain the velocities at time step $n = 1/2$ from pressures at $n = 0$ and prior velocities at $n = -1/2$. Then (4) is used to obtain the pressure at $n = 1$ from the velocities at $n = 1/2$ and the prior pressure at $n = 0$. Next (5) and (6) are used to update the velocities and the cycle is repeated for the desired number of time steps. Initially the fields are zero and hence known throughout the computational domain. Energy is introduced into the FDTD grid via the total-field/scattered-field (TF/SF) boundary as explained in Sec. 2.3. In a typical program, the "current" value of a field is calculated from the "old" and the old value is then overwritten with the current one. One advantage of the leap-frog method is that there is no need to store the entire history of the fields, nor is inversion of any matrices required.

While the numerical results presented are restricted to isovelocity cases, multiple velocities can easily be included in the FDTD method. The ability to readily model volume inhomogeneities is one of the major advantages of the FDTD method.

As discussed earlier and in [8], fields propagated by (4)-(6) suffer numerical dispersion. However, since only one frequency is of interest and most of the energy travels in a single direction, a correction factor can be found to compensate for most of the effects of the numerical dispersion. As discussed in [1], this correction factor is used to modify the wave number for both the incident field and the near-to-far field calculations so that they better agree with the fields propagating in the FDTD grid. This technique is used to obtain the results presented in this paper.

2.2 Local Conformal FDTD Method

The traditional FDTD method specifies media at discrete locations on a Cartesian grid. As a result, curved boundaries are modeled using a staircase approximation as shown in Fig. 1(a). The error associated with this approximation can be reduced by decreasing the grid spacing, but this can greatly increase the computational cost. An alternative approach is to use a conformal technique in which the grid is altered to conform to the curved boundaries. In this work, a local conformal technique is used which is based on the integral form of (1). This method is analogous to the dielectric-dielectric technique introduced by Jurgens *et al.* [2] for electromagnetic problems. However, our approach differs from the one used in [2] in that it includes reciprocal borrowing as discussed in [3]. Taking the volume integral of both sides of the continuity equation (i.e., the 3-D form of (1)) yields

$$\int_V \frac{\partial p}{\partial t}\, d\mathrm{V} = -\rho c^2 \int_V \nabla \cdot \vec{v}\, d\mathrm{V} \tag{10}$$

Using the divergence theorem $\int_v \nabla \cdot \vec{A} d\mathrm{V} = \oint_s \vec{A} \cdot \hat{n} ds$ and reducing to the 2-D case yields

$$\int_S \frac{\partial p}{\partial t}\, ds = -\rho c^2 \oint_l \vec{v} \cdot \hat{n}\, dl \tag{11}$$

where surface S and contour l are shown in Fig. 1(b) for two contours—one above the surface and the other below the surface. Quantities associated with the contour above the surface have a subscript 1, while those below have a subscript 2. The vector $\hat{n}$ is the outward unit normal vector along a specified contour. To obtain the update equations from (11) it is assumed that the pressure is constant over a given S and the normal component of the velocity is constant over each segment of the contour l. Thus, if a node is adjacent to the surface and above it, the update equation is given by

$$\begin{aligned} p^n(i,j) \quad &= \quad p^{n-1}(i,j) - \frac{\rho c^2 \Delta t}{\frac{1}{2}(l_{1a} + l_{1b})\delta} \Big(l_{1b} v_x^{n-1/2}(i+1/2,j) - \\ &\qquad l_{1a} v_x^{n-1/2}(i-1/2,j) + v_z^{n-1/2}(i,j+1/2) - l_s v_n \Big) \end{aligned} \tag{12}$$

and if the node is adjacent to the surface and below it, the update equation is given by

$$\begin{aligned} p^n(i,j) \quad &= \quad p^{n-1}(i,j) - \frac{\rho c^2 \Delta t}{\frac{1}{2}(l_{2a} + l_{2b})\delta} \Big(l_{2b} v_x^{n-1/2}(i+1/2,j) - \\ &\qquad l_{2a} v_x^{n-1/2}(i-1/2,j) - v_z^{n-1/2}(i,j-1/2) + l_s v_n \Big) \end{aligned} \tag{13}$$

where lengths l_{1a}, l_{1b}, l_{2a}, l_{2b}, and l_s are shown in Fig. 1(b). The normal component of the velocity v_n along the surface segment is shown in Fig. 1(a) and (c). The update equation for v_n is discussed below.

Figure 2 shows a special case in which the circled v_x node cannot be updated because its neighboring pressure nodes are in different media. Therefore, this v_x node cannot be used to update the surrounding pressure nodes. Instead, to update the pressure in S_a, the boxed v_x node above the surface is borrowed. Similarly, for the pressure in S_b, the boxed v_x node below the surface is used. This approach is consistent with that used in [2]. However, an additional step, reciprocal borrowing, is included which improves stability and accuracy. For example, consider the node v_{xb} below the surface in Fig. 2. Normally, this velocity node is updated using its neighboring pressures, p_2 and p_3. In reciprocal borrowing, p_2 is replaced by the weighted average $(l_1 p_1 + l_2 p_2)/(l_1 + l_2)$. If this modification were not used, the pressure p_1 would be affected by the velocity at v_{xb} (via the borrowing used by the circled node), but v_{xb} would not be directly affected by p_1. This non-reciprocal interaction of fields is non-physical and may lead to unstable behavior. (Nonreciprocal borrowing effectively introduces spurious energy into the computational domain. For closed problems, such as a resonant enclosure, this often leads to unstable behavior. However, for unbounded problems, such as the one considered here, spurious energy is less likely to result in instability, although this energy does represent an inherent error. For the numerical results presented in this paper, stability was not a problem.) Details on reciprocal borrowing can be found in [3] and [9].

The boundary condition at a fluid-fluid interface dictates that the velocity normal to the surface must be continuous. The calculation of v_n requires the integral forms of (2) and (3). Rewriting the 3-D equivalents of (2) and (3) as a single vector equation and taking the volume integral of both sides yields

$$\int_V \frac{\partial \vec{v}}{\partial t}\, d\mathrm{V} = -\frac{1}{\rho} \int_V \nabla p \, d\mathrm{V} \tag{14}$$

Using the identity $\int_v \nabla \phi \, d\mathrm{V} = \int_s \phi \hat{n} \, ds$ and reducing to the 2-D case yields

$$\int_S \frac{\partial v_x}{\partial t}\, ds = -\frac{1}{\rho} \oint_l p n_x \, dl \tag{15}$$

$$\int_S \frac{\partial v_z}{\partial t}\, ds = -\frac{1}{\rho} \oint_l p n_z \, dl \tag{16}$$

where n_x and n_z are the $x-$ and $z-$components of the outward unit normal (i.e., the unit vector points away from the interior defined by the closed path). Equation (16) may be modified to compute v_n by introducing a rotated auxiliary contour as shown in Fig. 1(c). For this contour, rotated coordinates x' and z' are introduced and (16) becomes

$$\int_{S'} \frac{\partial v_n}{\partial t}\, ds' = -\frac{1}{\rho} \oint_{l'} p n_{z'}\, dl' \tag{17}$$

where $v_{z'}$ has been replaced by v_n, and $n_{z'}$ is the outward normal projected in the z' direction. To obtain the update equation, it is assumed that v_n is constant over S' and that the pressure is constant over each segment of l'. The component $n_{z'}$ is nonzero only for segments parallel to the surface. The values for the pressures on these segments, indicated by p_{int1} and p_{int2} in Fig. 1(c), are obtained by interpolating between neighboring pressure nodes. The density ρ is referred to as ρ_1 above the surface and ρ_2 below. Under these assumptions, (17) yields the following update equation

$$v_n^{n+1/2} = v_n^{n-1/2} - \frac{\Delta t}{(d_1\rho_1 + d_2\rho_2)}(p_{\text{int1}} - p_{\text{int2}}) \tag{18}$$

where lengths d_1 and d_2 are shown in Fig. 1(c).

2.3 Problem Geometry and Absorbing Boundary Conditions

A total-field/scattered-field (TF/SF) formulation [10] is used to introduce the incident field into the FDTD grid. Alternative means of introducing energy into the computational domain are inclusion of the acoustic source within the grid or use of a scattered-field approach. For the problem at hand, the source is assumed to be far from the surface and hence cannot, in practice, be included in the grid. The scattered-field approach requires calculation of the incident field at each node throughout the bottom fluid and hence is less efficient than the TF/SF approach (which only requires calculation of the incident field over the boundary between the total-field and the scattered-field regions).

In the TF/SF approach a boundary typically separates a subsection of the grid, which includes all scatterers and contains total fields (incident plus scattered), from the rest of the grid, which contains only scattered fields. In this approach, the incident field is introduced along the boundary between the total-field and scattered-field regions. However, for the rough surface scattering problem considered here, it is not possible to surround the scatterer, i.e., the rough surface, completely by such a boundary. Instead, as shown in Fig. 3, a horizontal boundary is defined along a large section of the rough surface a few cells above its highest point. Near the left and right sides of the computational domain, this boundary "turns" downward, continues to the surface, and stops. The tapered incident field specified over this boundary is maximum at the center of the computational domain and falls off exponentially to either side. Thus, although the TF/SF boundary terminates abruptly at the ends of the rough surface and hence is not "physical," the fields introduced at these terminations are small and the spurious energy introduced into the grid has a negligible effect on the total scattering strength data.

Since the FDTD method is a time domain method, it is capable of providing broadband results from a single simulation. However, here we are interested in obtaining scattering strengths for a single frequency. Regardless of whether one is interested in a single frequency or a broad range of frequencies, the excitation of the FDTD grid must be "switched on." Hence, there are always some transients associated with the start of the simulation. As discussed in [1], the magnitude of the transient can be reduced by gradually increasing the incident field magnitude. Once the transients are no longer significant, the magnitude and phase of the fields are determined over the boundary identified as the "data collection zone" in Fig. 3. This zone is located two grid cells above the highest elevation of the surface. When steady state has been achieved, two samples (in time) of a field at each point along the zone are sufficient to determine the corresponding magnitude and phase. These near-field values are subsequently transformed to the far field, as discussed in [4], to obtain the scattering strength. The transformation is an application of Huygens' principle with the use of the large-argument approximation of the Green's function to simplify the calculation.

For unbounded problems, the FDTD method requires absorbing boundary conditions (ABCs) to terminate the computational domain. If ABCs are not used, the problem is bounded by the termination of the computational domain which acts like a perfect reflector. In this work, the perfectly matched layer (PML) ABC [11] was used to surround the computational domain as shown in Fig. 3. Ideally, ABCs completely absorb outgoing waves that impinge on the edges of the computational domain. However, since ABCs are imperfect, some nonphysical reflection remains. In some cases, the amount of spurious energy introduced by the ABC can be reduced by adding space between the ABC and the scatterer. For this work, a buffer of 48 grid spaces is used between the upper portion of the PML and the surface maximum. (The field is sampled at 32 points per wavelength in water so that the distance from the highest point of the surface to the edge of the PML is 1.5 wavelengths.) Spurious reflections originating below the surface lose energy when they pass through the surface. Hence, their effect on the fields gathered above the surface is reduced. For this reason, a buffer of only 16 grid cells was used between the lower portion of the PML and the surface minimum.

3 Numerical Results

To test the accuracy of the FDTD method for a water-sediment interface, three different cases were examined. Two of these were for a mud sediment, which has a slower compressional speed than water, and one was for a silty-clay sediment, which has a faster compressional speed. Shear speeds for both bottom types are negligible. For the mud cases, a Gaussian spectrum was used. The Gaussian spectrum is useful because it can provide a more stringent test at low grazing angles in the backward scattering direction where scattering levels can be relatively low, particularly as the correlation length is increased. In addition, the Gaussian spectrum is sometimes used when the accuracy of an approximate model is first examined. For the silty-clay case, a modified power law (MPL) spectrum was used. The MPL spectrum is more realistic for shallow water sediment bottoms than the Gaussian spectrum; the former represents multiscale roughness, while the latter represents single-scale roughness. The Gaussian spectrum is given by

$$W(K) = \frac{h^2 l}{2\sqrt{\pi}} e^{-K^2 l^2/4} \tag{19}$$

where h is the rms surface height and l is the surface correlation length, and the MPL spectrum is given by

$$W(K) = \frac{w_1}{K^2 + K_L^2} \tag{20}$$

where w_1 is a strength parameter and K_L is the cut-off spatial wave number given by $\pi w_1/h^2$.

For simplicity, attenuation in the sediment is not included in any of the three test cases. The method used to generate finite-length surface realizations and the source function used for the incident field are explained in [12]. To facilitate comparison of the FDTD results with those of the IE approach the same sets of surfaces are used to obtain the results for both methods. The dimensionless parameters kh and kl, where k is the wave number in the water, are used for the Gaussian spectrum results. The statistical parameters chosen for the modified power law results are consistent with an insonification frequency of 7.5 kHz. An incident angle of $70°$ measured from the vertical is used for all three cases.

The integral equation method for the two-fluid boundary is closely analogous to the integral equation method for electromagnetic scattering at a rough surface separating two media (see Appendix A). A detailed exposition for the electromagnetic case is given in [13], and the simpler case of a single fluid with a rough surface subject to a Dirichlet boundary condition is treated in [12]. With a specified incident pressure field on the rough surface, solution of the integral equation (actually two coupled integral equations) for the two-fluid interface gives the pressure field and the normal derivative of the pressure field on the surface. With these quantities known, the pressure is transformed to the far field to obtain the scattering strength in a manner analogous to that used for the FDTD method.

To obtain accurate results over all scattering angles using the FDTD conformal method, 32 points per wavelength were required. Cases run without the conformal method, i.e., using a staircase representation of the surface, indicated that a finer discretization is needed to obtain results of comparable quality. While 32 points per wavelength might seem large, the results presented include backscattering at low grazing angles, a regime that is not typically considered since at low grazing angles backscattering levels are quite low.

Two different results are shown for the test cases. The first result is for a single surface realization. This allows a close examination of any differences between the results for both the FDTD and IE methods. The second result is for a Monte Carlo average of scattering strengths obtained for fifty different surface realizations. The Monte Carlo averages are of interest since they are used to benchmark approximate methods for which formal averages for the scattering cross sections have been obtained.

In our first test case, a Gaussian spectrum is used, and the values for the parameters kh and kl are 0.6 and 4.0, respectively. The environmental parameters are for mud and water from measurements made in the Adriatic Sea in 1990 [14]. They are the speed of sound in water $c_{water} = 1505.5$ m/s, the density of water $\rho_{water} = 1000$ kg/m^3, the speed of sound in the mud $c_{sediment} = 1478$ m/s, and the density of the mud $\rho_{sediment} = 1620$ kg/m^3. The incident angle is 70°. For the single-surface result shown in Fig. 4(a), discrepancies occur between the IE and FDTD values at low grazing angles. Low grazing angles are the most challenging for the FDTD method since any imperfections in the absorbing boundary conditions will be most apparent in these regions. There are also some differences in the values of the minima, but these are almost certainly due to differences in sampling. For the FDTD method, values were obtained at every tenth of a degree; for the IE method, values were obtained at every quarter of a degree. The Monte Carlo average for fifty surface realizations, Fig. 4(b), shows virtually no differences between the two methods except at low grazing angles where the differences are barely perceptible.

The same environmental parameters are used for the second test case, but kh is tripled to 1.8 and kl is doubled to 8.0. For kl this large, the values of the scattering strength drop off rapidly in the backscattering direction. Again the single surface results for the FDTD, Fig. 5, differ from those of the IE method only at grazing angles, although the differences are somewhat larger than for the first test case. The same is true for the Monte Carlo results, not shown here.

For the third test case, the modified power law spectrum is used with $w_1 = 0.02$ cm and $K_L = 6.981317 \times 10^{-3}$ m^{-1}. The rms surface height is 3 cm, the frequency is 7.5 kHz, and again the incident angle is 70°. The environmental parameters are for silty-clay and water from measurements made in Tellero, Italy, in 1988 [14]. The speed of sound in water is $c_{water} = 1521.8$ m/s, the density of water is $\rho_{water} = 1000$ kg/m^3, the speed of sound in the silty-clay is $c_{sediment} = 1537$ m/s, and the density of the silty-clay is $\rho_{sediment} = 1770$ kg/m^3. For the single-surface result, Fig. 6(a), deviations between the IE and FDTD values appear to be greater, but the Monte Carlo average results, Fig. 6(b), are virtually the same. The latter is probably because of the higher values of the scattering strength characteristic of power law spectra which are not as greatly affected by imperfections in the absorbing boundary conditions.

4 Summary

A modified finite-difference time-domain (FDTD) method is described for calculating acoustic scattering from one-dimensional fluid-fluid interfaces modeling water-sediment interfaces. The FDTD method is used to solve coupled differential equations. Numerical results are presented for scattering from single surface realizations and for averages of scattering from an ensemble of surfaces—that is, for Monte Carlo averages—for both a Gaussian spectrum and a modified power law spectrum. These results are compared with those obtained using an integral equation technique and agree well over all scattering angles indicating that both methods can be used to obtain accurate results for fluid-fluid interfaces. For the results presented here, the integral equation results are more straightforward and readily obtained, but the advantage of the FDTD method over the integral equation approach is that complex geometries do not appreciably increase the cost or difficulty of its implementation. Also, while only a single frequency is considered in this work, another of the FDTD method's advantages is that it can be used to obtain broadband results.

A. Coupled Integral Equations for the Two-Fluid Interface

In [13], coupled integral equations for a p-polarized electromagnetic field incident on a dielectric rough surface are given by Eqs. (3.32) and (3.33) or by Eqs. (3.49a) and (3.49b). The coupled integral equations for an acoustic pressure field incident on a rough two-fluid interface can be obtained from the equations in [13] using the following associations: The total pressure field, $p(\mathbf{r})$, on the rough surface is analogous to the magnetic field, $H(x_1|\omega)$, in [13]. The quantity

$$\left(-\frac{df(x)}{dx}\frac{\partial}{\partial x}+\frac{\partial}{\partial z}\right)p(\mathbf{r})=0$$

on the rough surface, which is proportional to the normal derivative of the total pressure field on the rough surface, with $f(x)$ the rough surface profile, is analogous to $L(x_1|\omega)$ in [13]. Finally, the density ratio of the two fluids, ρ_2/ρ_1, where the field is incident on the side with density ρ_1 is analogous to the dielectric constant $\epsilon(\omega)$ in [13].

References

[1] F. D. Hastings, J. B. Schneider, and S. L. Broschat, "A finite-difference time-domain solution to scattering from a rough pressure-release surface," *Journal of the Acoustical Society of America*, vol. 102, pp. 3394–3400, Dec. 1997.

[2] T. G. Jurgens, A. Taflove, K. Umashankar, and T. G. Moore, "Finite-difference time-domain modeling of curved surfaces," *IEEE Transactions on Antennas and Propagation*, vol. 40, pp. 357–366, Apr. 1992.

[3] C. J. Railton, I. J. Craddock, and J. B. Schneider, "An improved locally distorted CPFDTD algorithm with provable stability," *Electronics Letters*, vol. 31, no. 18, pp. 1585–1586, 1995.

[4] F. D. Hastings, J. B. Schneider, and S. L. Broschat, "A Monte-Carlo FDTD technique for rough surface scattering," *IEEE Transactions on Antennas and Propagation*, vol. 43, pp. 1183–1191, Nov. 1995.

[5] D. Botteldooren, “Acoustical finite-difference time-domain simulation in a quasi-Cartesian grid,” *Journal of the Acoustical Society of America*, vol. 95, pp. 2313–2319, May 1994.

[6] J. LoVetri, D. Mardare, and G. Soulodre, “Modeling of the seat dip effect using the finite-difference time-domain method,” *J. Acoust. Soc. Am.*, vol. 100, pp. 2204–2212, Oct. 1996.

[7] J. G. Maloney and K. E. Cummings, “Adaptation of FDTD techniques to acoustic modeling,” in *11th Annual Review of Progress in Applied Computational Electromagnetics*, vol. 2, (Monterey, CA), pp. 724–731, Mar. 1995.

[8] A. Taflove, “Review of the formulation and applications of the finite-difference time-domain method for numerical modeling of electromagnetic wave interactions with arbitrary structures,” *Wave Motion*, vol. 10, no. 6, pp. 547–582, 1988.

[9] C. J. Railton and I. J. Craddock, “Stabilised CPFDTD algorithm for the analysis of arbitrary 3D PEC structures,” *IEE Proceedings H: Microwaves, Antennas and Propagation*, vol. 143, pp. 367–372, Oct. 1996.

[10] A. Taflove, *Computational Electrodynamics: The Finite-Difference Time-Domain Method.* Boston, MA: Artech House, 1995.

[11] J.-P. Berenger, “A perfectly matched layer for the absorption of electromagnetic waves,” *Journal of Computational Physics*, vol. 114, no. 1, pp. 185–200, 1994.

[12] E. I. Thorsos, “The validity of the Kirchhoff approximation for rough surface scattering using a Gaussian roughness spectrum,” *J. Acoust. Soc. Am.*, vol. 83, no. 1, pp. 78–92, 1988.

[13] A. A. Maradudin, T. Michel, A. R. McGurn, and E. R. Mendez, “Enhanced backscattering of light from a random grating,” *Annals of Physics*, vol. 203, pp. 255–307, 1990.

[14] M. D. Richardson, “In-situ, shallow-water sediment geoacoustic properties,” in *Proceedings of the 1997 International Conference on Shallow-Water Acoustics*, (Beijing, China), pp. 163–170, Apr. 1997.

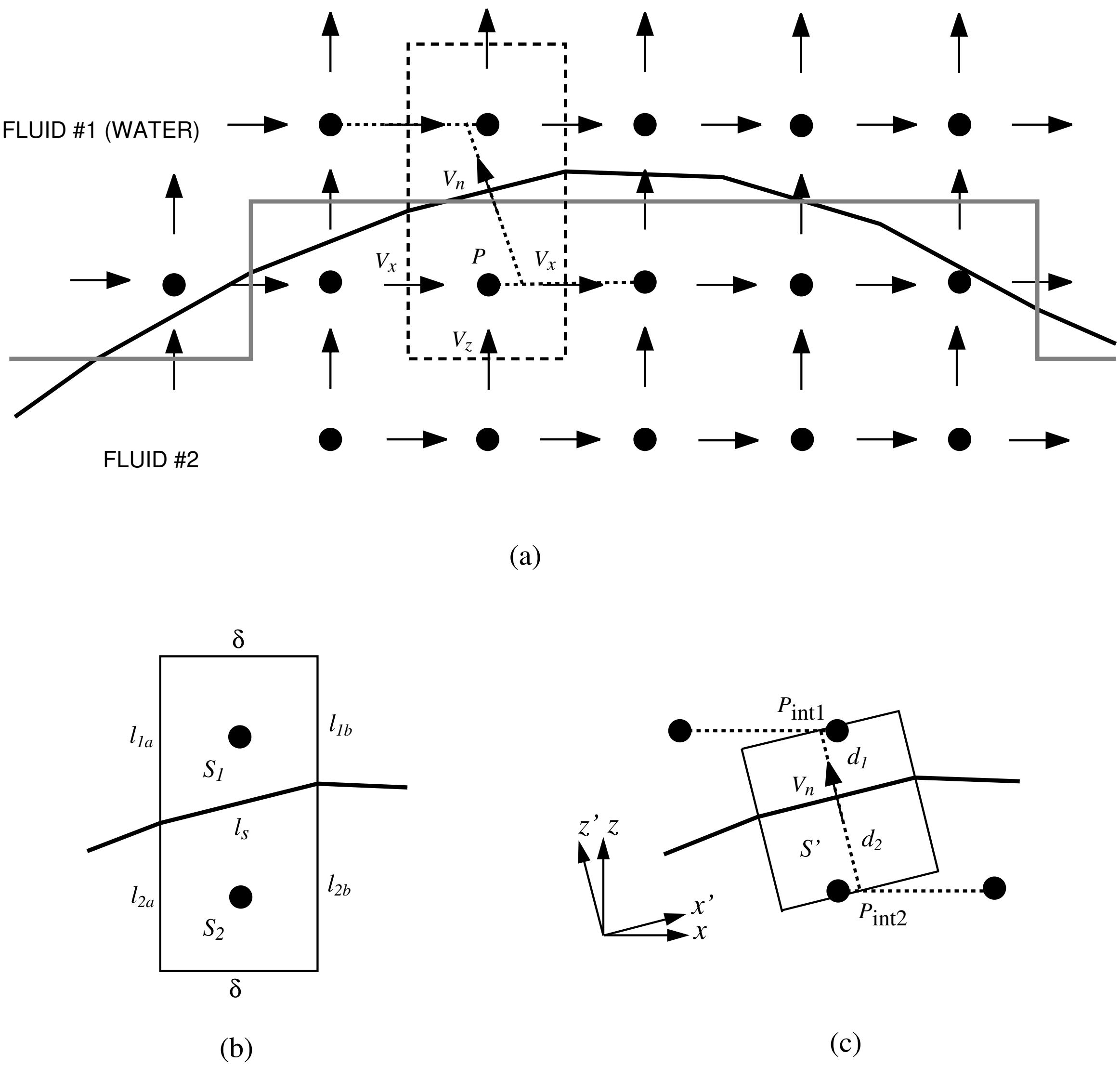

Figure 1: (a) Actual surface (solid black line) and staircase approximation (solid gray line). Circles correspond to pressure nodes and arrows correspond to velocity nodes. (b) Contours used to compute pressures in conformal cells adjacent to the surface. The width of the cells are δ and the heights are such that $l_{1a} + l_{2a} = l_{1b} + l_{2b} = 2\delta$. (c) Auxiliary contour for computing normal velocity from interpolated pressures.

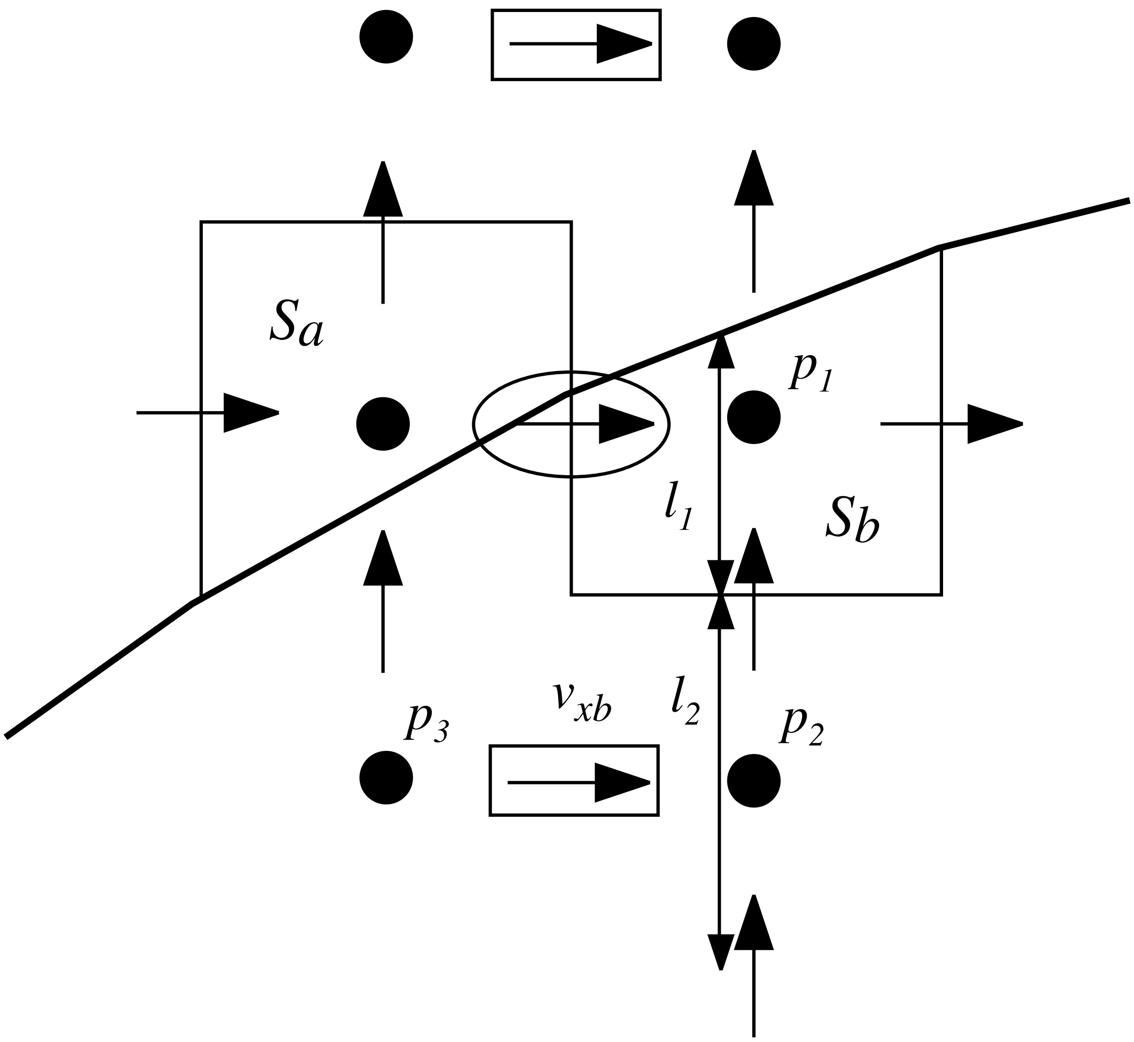

Figure 2: Geometry for reciprocal borrowing. The circled v_x node is unused. The boxed v_x's above and below the surface are used for the pressure update in cells S_a and S_b, respectively. A weighted average of p_1 and p_2 is used to update v_{xb}.

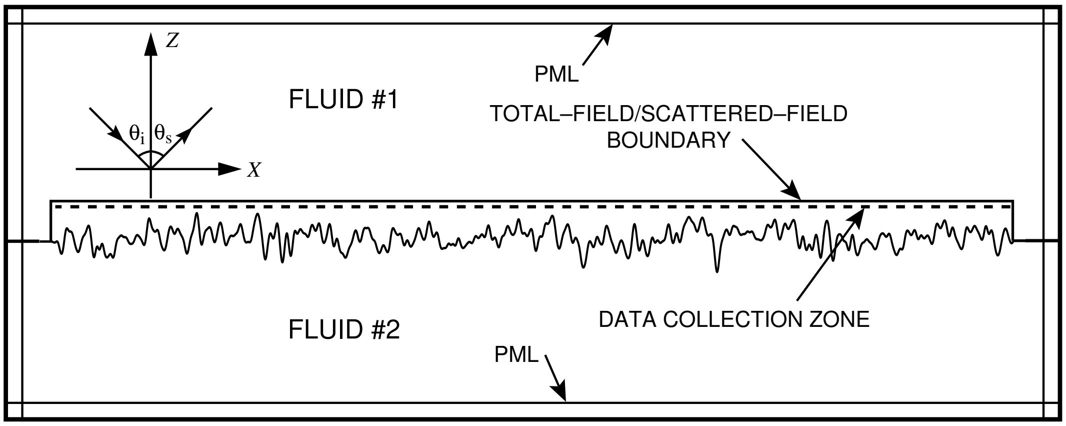

Figure 3: FDTD computational domain. Near-field data is measured along the data collection zone (dashed line). The total-field region is below the solid line and includes the rough surface. The perfectly matched layer (PML) absorbing boundary condition terminates the domain. Incident and scattering angles are measured from the vertical. Figure is not to scale.

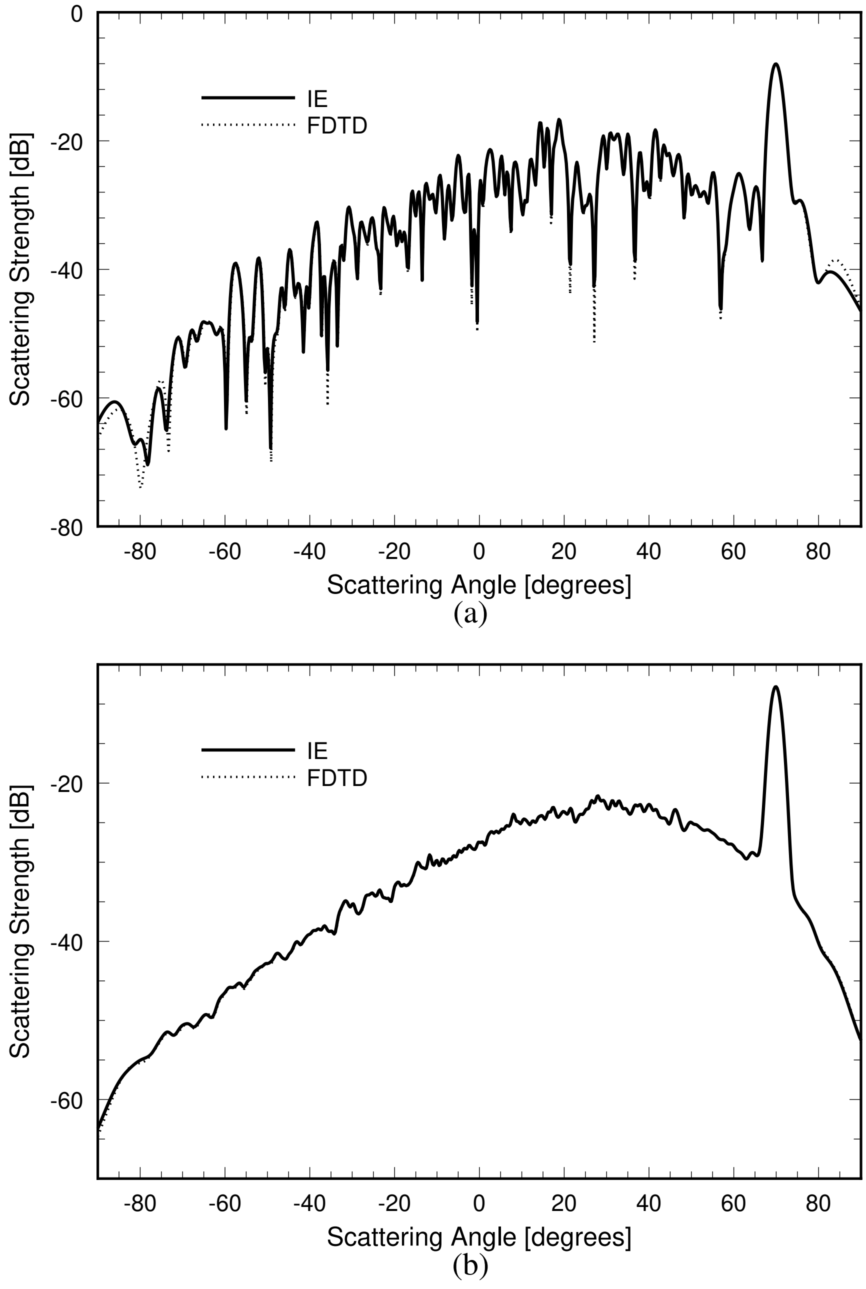

(a)

(b)

Figure 4: Scattering strength from a surface with a Gaussian roughness spectrum: $kh = 0.6$ and $kl = 4.0$. Incident angle is $70°$ from vertical. The water and sediment have the following parameters: $c_{water} = 1505.5$ m/s, $\rho_{water} = 1000$ kg/m^3, $c_{sediment} = 1478$ m/s, and $\rho_{sediment} = 1620$ kg/m^3. (a) Single surface realization. (b) Monte Carlo average over 50 surface realizations.

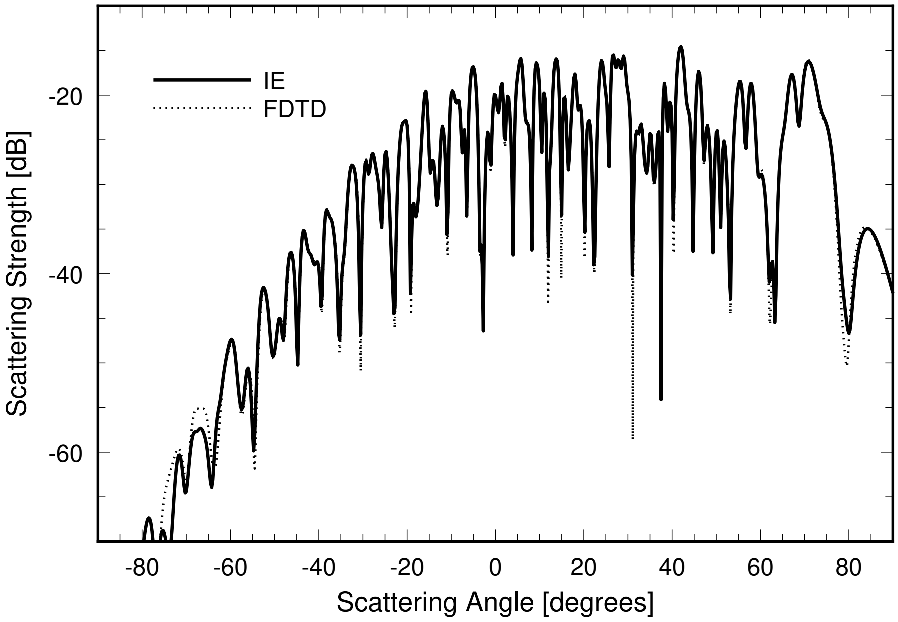

Figure 5: Scattering strength from a surface with a Gaussian roughness spectrum: $kh = 1.6$ and $kl = 8.0$. All other parameters are the same as for the previous figure.

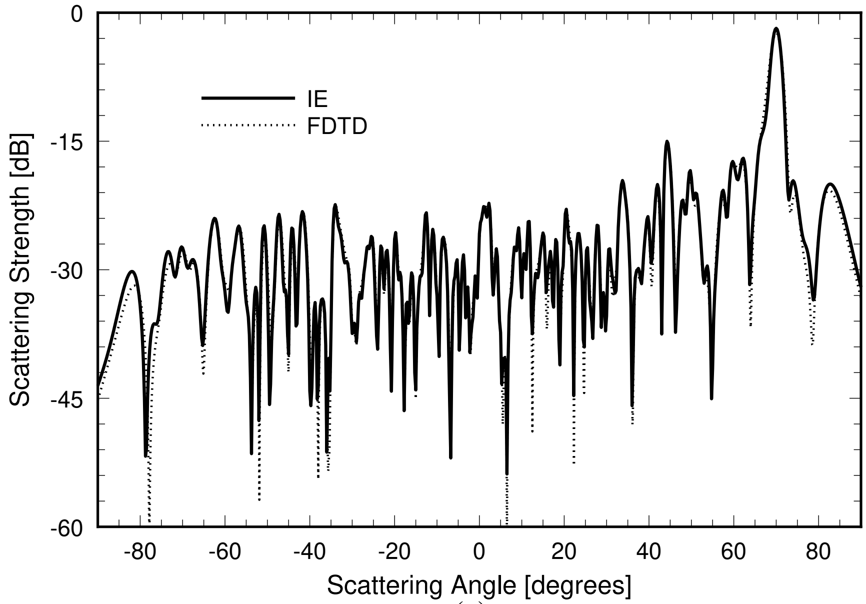

(a)

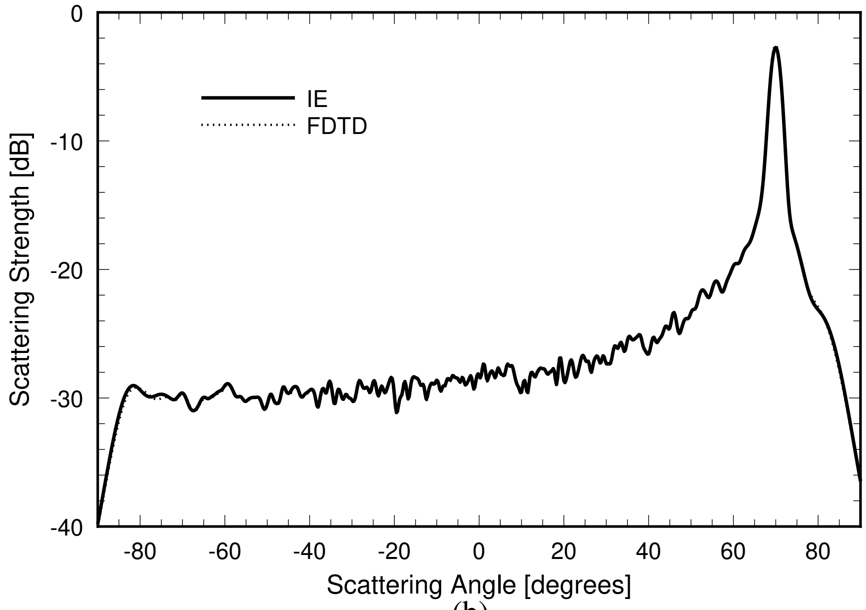

(b)

Figure 6: Scattering strength from a surface with a modified power law roughness spectrum: $w_1 = 0.02$ cm, $K_L = 6.981317 \times 10^{-3}$ m^{-1}, $h = 3$ cm, the frequency is 7.5 kHz. Incident angle is 70° from vertical. The water and sediment have the following parameters: $c_{water} = 1521.8$ m/s, $\rho_{water} = 1000$ kg/m^3, $c_{sediment} = 1537$ m/s, and $\rho_{sediment} = 1770$ kg/m^3. (a) Single surface realization. (b) Monte Carlo average over 50 surface realizations.